Periodic Trends in the Binding of Metal Ions to Pyrimidine Studied by Threshold Collision-Induced Dissociation and Density Functional Theory

R. Amunugama and M. T. Rodgers*

Department of Chemistry, Wayne State University, Detroit, Michigan 48202

Received: February 21, 2001; In Final Form: July 30, 2001

Threshold collision-induced dissociation of M^+(pyrimidine) with xenon is studied using guided ion beam tandem mass spectrometry. M^+ includes the following metal ions: Mg^+, Al^+, Sc^+, Ti^+, V^+, Cr^+, Mn^+, Fe^+, Co^+, Ni^+, Cu^+, and Zn^+. In all cases, the primary product corresponds to endothermic loss of the intact pyrimidine molecule, with minor production of MXe^+ formed by ligand exchange. Additional minor reaction pathways, the result of a $M^+(Ar)_2$ isobaric contaminant, are observed in several systems (Fe^+, Co^+, and Ni^+). The cross-section thresholds are interpreted to yield 0 and 298 K bond dissociation energies for M^+−pyrimidine after accounting for the effects of multiple ion-molecule collisions, internal energy of the reactant ions, and dissociation lifetimes. Density functional calculations at the B3LYP/6-31G* level of theory are used to determine the structures of these complexes and provide molecular constants necessary for the thermodynamic analysis of the experimental data. Theoretical bond dissociation energies are determined from single point calculations at the B3LYP/6-311+G(2d,2p) level using the B3LYP/6-31G* optimized geometries. Excellent agreement between theory and experiment is found for the Mg^+, Al^+, Sc^+, Mn^+, $Fe^+(^6D)$, Co^+, Ni^+, and Zn^+, whereas the theoretical bond dissociation energies to Ti^+, V^+, Cr^+, $Fe^+(^4F)$, and Cu^+ lie outside of the experimental error bars. Trends in the binding energies of pyrimidine show behavior similar to that observed for ammonia and pyridine.

Introduction

Studies of the interactions between gas-phase metal ions and biologically relevant small molecules continue to attract the attention of both experimentalists and theoreticians because such studies reveal useful insights into the properties of these interactions in the absence of solvation. An area that has seen a flurry of activity relates to studies directed toward an understanding of metal ion-nucleic acid interactions. Motivation for such studies comes from the fact that metal ions participate in all biological processes that involve nucleic acids. The role of metal ions in determining the structure and functioning of nucleic acids is influenced by the site at which binding occurs, and the effects of metal ion binding vary from stabilization of the three-dimensional structure to transcription failure and even cell death. The presence, identity, and location of metal ions strongly influence the conformation of a nucleic acid, which in turn controls the activity of nucleic acids. Nonspecific binding of metal ions to the phosphate backbone gives rise to stabilization of the double helix through neutralization of the negative charges residing on the phosphate backbone. Binding of a metal ion to the base also neutralizes the negative charge on the phosphate backbone through a zwitterion effect, but can interfere with hydrogen bonding and stacking interactions between bases. Such metal ion-base interactions may destabilize the helix. Erroneous pairing and subsequent transcription errors may occur if the metal ion interferes with base-base interactions. Therefore, the course of genetic information transfer may be altered by metal ion-nucleic acid interactions.

Metal ions that are hard and have a low tendency to form covalent bonds, such as the alkali ions and Mg^{2+}, tend to bind to the phosphate backbone. Other metal ions, such as transition metal ions, have a greater likelihood to form covalent bonds and are softer than the alkali metal ions. Competition between the phosphate backbone and the bases for binding of transition metal ions is therefore much more likely. An understanding of the interaction of various metal ions with nucleic acids is thus essential to understand the role and effects of metal ions in their biological activity.

In recent work, we have developed methods to allow the application of quantitative threshold collision-induced dissociation methods to obtain accurate thermodynamic information on increasingly large systems.[1−10] One of the driving forces behind these developments is our interest in applying such techniques to systems having biological relevance. In addition, we seek to perform accurate thermochemical measurements that provide absolute anchors for metal cation affinity scales over an ever-broadening range of energies. In the present paper, we examine the interactions of pyrimidine with a variety of metal ions. The structure of pyrimidine is shown in Figure 1 along with its calculated[11] and measured[12] dipole moments and estimated polarizability.[13] Pyrimidine was chosen as a simple model of noncovalent interaction with metal ions for a wide variety of nitrogen-containing heterocycles of biological importance and, of particular interest, the nucleic acid bases.

Pyrimidines play a wide variety of roles in biochemical systems. They are the building blocks of the nucleic acids, as well as vitamin B_1, folic acid, barbiturates, antimalarials, oral diuretics, and other pharmaceuticals. They fulfill a series of important functions in biochemical oxidation-reduction processes. They act as dehydrogenases, as one- and two-electron-transfer reagents, and as activators of molecular O_2. The interaction of pyrimidines with cations is particularly important as σ coordination and π redox reactivity may influence one another.[14]

10.1021/jp010663i CCC: $20.00
Published on Web 10/03/2001

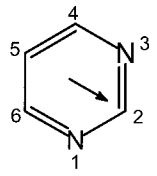

pyrimidine
2.33 D (2.31 D)
8.61 Å3

Figure 1. Structure of the pyrimidine molecule. The dipole moment is shown as an arrow. Values for the dipole moment are taken from theory[11] and experiment,[12] listed in parentheses. The estimated polarizability is also shown.[13]

In the present study, we use guided ion beam mass spectrometry to collisionally excite complexes of M^+ bound to pyrimidine, where $M^+ = Mg^+$, Al^+, Sc^+, Ti^+, V^+, Cr^+, Mn^+, Fe^+, Co^+, Ni^+, Cu^+, and Zn^+. The kinetic energy-dependent cross sections for the collision-induced dissociation (CID) processes are analyzed using methods developed previously.[3] The analysis explicitly includes the effects of the internal and translational energy distributions of the reactants, multiple collisions, and the lifetime for dissociation. We derive metal cation-pyrimidine bond dissociation energies (BDEs) for all of the complexes, and compare these results to the theoretical values determined here and those in the literature.[7,11,15,16]

Experimental Section

General Procedures. Cross sections for CID of M^+(pyrimidine), where $M^+ = Mg^+$, Al^+, Sc^+, Ti^+, V^+, Cr^+, Mn^+, Fe^+, Co^+, Ni^+, Cu^+, and Zn^+ are measured using a guided ion beam mass spectrometer that has been described in detail previously.[17,18] The metal-ligand complexes are generated as described below. The ions are extracted from the source, accelerated, and focused into a magnetic sector momentum analyzer for mass analysis. Mass-selected ions are decelerated to a desired kinetic energy and focused into an octopole ion guide, which traps the ions in the radial direction.[19] The octopole passes through a static gas cell containing xenon, used as the collision gas, for reasons described elsewhere.[20−22] Low gas pressures in the cell (typically 0.05−0.20 mTorr) are used to ensure that multiple ion-molecule collisions are improbable. Product and unreacted beam ions drift to the end of the octopole where they are focused into a quadrupole mass filter for mass analysis and subsequently detected with a secondary electron scintillation detector and standard pulse counting techniques.

Ion intensities are converted to absolute cross sections as described previously.[17] Absolute uncertainties in cross section magnitudes are estimated to be ±20%, which is largely the result of errors in the pressure measurement and the length of the interaction region. Relative uncertainties are approximately ±5%.

Ion kinetic energies in the laboratory frame, E_{lab}, are converted to energies in the center of mass frame, E_{CM}, using the formula $E_{CM} = E_{lab}m/(m + M)$, where M and m are the masses of the ionic and neutral reactants, respectively. All energies reported below are in the CM frame unless otherwise noted. The absolute zero and distribution of the ion kinetic energies are determined using the octopole ion guide as a retarding potential analyzer as previously described.[17] The distribution of ion kinetic energies is nearly Gaussian with a fwhm typically between 0.2 and 0.3 eV (lab) for these experiments. The uncertainty in the absolute energy scale is ±0.05 eV (lab).

Even when the pressure of the reactant neutral is low, it has previously been demonstrated that the effects of multiple collisions can significantly influence the shape of CID cross sections.[23] Because the presence and magnitude of these pressure effects is difficult to predict, we have performed pressure-dependent studies of all cross sections examined here. In the present systems, we observe small cross sections at low energies that have an obvious dependence upon pressure. We attribute this to multiple energizing collisions that lead to an enhanced probability of dissociation below threshold as a result of the longer residence time of these slower moving ions. Data free from pressure effects are obtained by extrapolating to zero reactant pressure, as described previously.[23] Thus, results reported below are due to single bimolecular encounters.

Ion Source. The M^+(pyrimidine) complexes are formed in a 1 m long flow tube[18,24] operating at a pressure of 0.7−0.8 Torr with a helium flow rate of approximately 4000−7000 sccm. Metal ions are generated in a continuous dc discharge by argon ion sputtering of a cathode, made from the metal of interest, or a tantalum "boat" containing a powder or crimpings of the metal of interest. Operating conditions of the discharge are 2−2.5 kV and 18−27 mA in a flow of roughly 10% argon in helium for the experiments performed here. The M^+(pyrimidine) complexes are formed by associative reactions of the metal ion with the neutral pyrimidine, which is introduced into the flow 50 cm downstream from the dc discharge. The complexes thus formed encounter in excess of 10^5 collisions with the bath gases, while traversing the remainder of the length of the flow tube. These conditions should thermalize the ions both vibrationally and rotationally. In our analysis of the data, we assume that the ions produced in this source are in their ground electronic states and that the internal energy of the M^+(pyrimidine) complexes is well described by a Maxwell-Boltzmann distribution of ro-vibrational states at 300 K. Previous work has shown that these assumptions are generally valid.[20,23−27]

Thermochemical Analysis. The threshold regions of the reaction cross sections are modeled using eq 1,

$$\sigma(E) = \sigma_0 \sum_i g_i (E + E_i - E_0)^n / E \qquad (1)$$

where σ_0 is an energy-independent scaling factor, E is the relative translational energy of the reactants, E_0 is the threshold for reaction of the ground electronic and ro-vibrational state, and n is an adjustable parameter. The summation is over the ro-vibrational states of the reactant ions, i, where E_i is the excitation energy of each state and g_i, is the population of those states ($\Sigma g_i = 1$). The populations of excited ro-vibrational levels are not negligible even at 300 K as a result of the many low-frequency modes present in these ions. The relative reactivity of all ro-vibrational states, as reflected by σ_0 and n, is assumed to be equivalent.

To obtain model structures and vibrational frequencies for the neutral and metalated pyrimidine, density functional theory calculations were performed using *Gaussian98*.[28] Geometry optimizations were performed at the B3LYP/6-31G* level. In the calculations performed for all of the complexes, the spin state was assumed to be the same as the ground state for the bare metal ion (i.e. Mg^+ doublet, Al^+ singlet, Sc^+ triplet, Ti^+ quartet, V^+ quintet, Cr^+ sextet, Mn^+ septet, Co^+ triplet, Ni^+ doublet, Cu^+ singlet, and Zn^+ doublet), except for Fe^+ where calculations were performed for both the sextet ground state and the quartet first excited state. Vibrational analyses of the geometry-optimized structures were performed to determine the vibrational frequencies of the reactant ions and product mol-

ecules. When used to model the data or to calculate thermal energy corrections, the B3LYP/6-31G* vibrational frequencies are scaled by a factor of 0.9804.[29] The scaled vibrational frequencies thus obtained for the 12 systems studied are available in Table S1 in Supporting Information, whereas Table S2 lists the rotational constants obtained from the geometry-optimized structures.

The Beyer-Swinehart algorithm[30] is used to evaluate the density of the ro-vibrational states, and the relative populations g_i are calculated by an appropriate Maxwell-Boltzmann distribution at the 300 K temperature appropriate for the reactants. The average vibrational energy at 298 K of the metal ion-bound pyrimidine is also given in Table S1. We have estimated the sensitivity of our analysis to the deviations from the true frequencies by scaling the calculated frequencies to encompass the range of average valence coordinate scale factors needed to bring calculated frequencies into agreement with experimentally determined frequencies found by Pople et al.[31] Thus, the originally calculated vibrational frequencies were increased and decreased by 10%. The corresponding change in the average vibrational energy is taken to be an estimate of one standard deviation of the uncertainty in vibrational energy (Table S1) and is included in the uncertainties listed with the E_0 values.

We also consider the possibility that collisionally activated complex ions do not dissociate on the time scale of our experiment (about 10^{-4} s) by including statistical theories for unimolecular dissociation into eq 1 as described in detail elsewhere.[3,25] This requires sets of ro-vibrational frequencies appropriate for the energized molecules and the transition states (TSs) leading to dissociation. The former are given in Tables S1 and S2, while we assume that the TSs are loose and product-like because the interaction between the metal ion and the pyrimidine ligand is largely electrostatic. In this case, the TS vibrations used are the frequencies corresponding to the products, which are also found in Table S1. The transitional frequencies, those that become rotations of the completely dissociated products, are treated as rotors, a treatment that corresponds to a phase space limit (PSL) and is described in detail elsewhere.[3] For the M^+(pyrimidine) complexes, the two transitional mode rotors have rotational constants equal to those of the neutral pyrimidine product with axes perpendicular to the reaction coordinate. These are listed in Table S2. The external rotations of the energized molecule and TS are also included in the modeling of the CID data. The external rotational constants of the TS are determined by assuming that the TS occurs at the centrifugal barrier for interaction of M^+ with the neutral pyrimidine ligand, calculated variationally as outlined elsewhere.[3] The 2-D external rotations are treated adiabatically but with centrifugal effects included, consistent with the discussion of Waage and Rabinovitch.[32] In the present work, the adiabatic 2-D rotational energy is treated using a statistical distribution with explicit summation over the possible values of the rotational quantum number, as described in detail elsewhere.[3]

The model represented by eq 1 is expected to be appropriate for translationally-driven reactions[33] and has been found to reproduce reaction cross sections well in a number of previous studies of both atom-diatom and polyatomic reactions,[34,35] including CID processes.[1,2,20,23−25,36−38] The model is convoluted with the kinetic energy distributions of both reactants, and a nonlinear least-squares analysis of the data is performed to give optimized values for the parameters σ_0, E_0, and n. The error associated with the measurement of E_0 is estimated from the range of threshold values determined for different data sets,

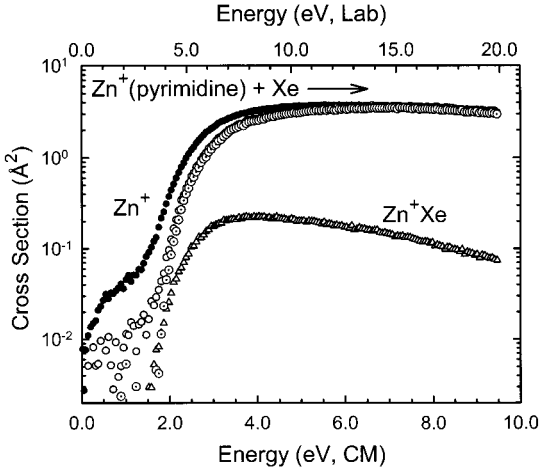

Figure 2. Cross sections for the collision-induced dissociation of the Zn^+(pyrimidine) complex with Xe as a function of the center-of-mass frame collision energy (lower *x*-axis) and laboratory frame (upper *x*-axis). Data for the Zn^+ product channel are shown for a Xe pressure of ~0.2 mTorr (●), extrapolated to zero (○), and after subtraction of the low-energy feature (⊙). The cross section for the ligand exchange process to form Zn^+Xe is also shown (△).

variations associated with uncertainties in the vibrational frequencies, and the error in the absolute energy scale, 0.05 eV (lab). For analyses that include the RRKM lifetime effect, the uncertainties in the reported E_0 values also include the effects of increasing and decreasing the time assumed available for dissociation (or equivalently, the distance traveled between the collision and detection) by a factor of two.

Equation 1 explicitly includes the internal energy of the ion, E_i. All energy available is treated statistically, which should be a reasonable assumption because the internal (rotational and vibrational) energy of the reactants is redistributed throughout the ion upon impact with the collision gas. The threshold for dissociation is by definition the minimum energy required leading to dissociation and thus corresponds to formation of products with no internal excitation. The assumption that products formed at threshold have an internal temperature of 0 K has been tested for several systems.[1,2,20,23−25] It has also been shown that treating all energy of the ion (vibrational, rotational, and translational) as capable of coupling into the dissociation coordinate leads to reasonable thermochemistry. The threshold energies for dissociation reactions determined by analysis with eq 1 are converted to 0 K bond energies by assuming that E_0 represents the energy difference between reactants and products at 0 K.[39] This assumption requires that there are no activation barriers in excess of the endothermicity of dissociation. This is generally true for ion-molecule reactions[34] and should be valid for the simple heterolytic bond fission reactions examined here.[40]

Results

Cross Sections for Collision-Induced Dissociation. Experimental cross sections were obtained for the interaction of Xe with 12 M^+(pyrimidine) complexes, where $M^+ = Mg^+$, Al^+, Sc^+, Ti^+, V^+, Cr^+, Mn^+, Fe^+, Co^+, Ni^+, Cu^+, and Zn^+. Figure 2 shows representative data for the Zn^+(pyrimidine) complex. Results for all 12 metal ions are available in Supporting Information (Figure S1). The most favorable process for all complexes is the loss of the intact pyrimidine molecule in the collision-induced dissociation, reactions 2.

$$M^+(\text{pyrimidine}) + Xe \rightarrow M^+ + \text{pyrimidine} + Xe \quad (2)$$

TABLE 1: Modeling Parameters of Eq 1 and Entropies of Activation at 1000 K of M^+(pyrimidine)[a]

M^+	σ_0[b]	n[b]	E_0[c] (eV)	E_0(PSL) (eV)	kinetic shift (eV)	ΔS(PSL) (J mol^{-1} K^{-1})
Mg^+	15.0 (0.3)	1.2 (0.1)	1.83 (0.05)	1.80 (0.06)	0.03	31 (3)
Al^+	11.2 (0.5)	1.3 (0.1)	1.67 (0.05)	1.65 (0.06)	0.02	30 (3)
Sc^+	3.0 (0.2)	1.2 (0.1)	2.37 (0.07)	2.22 (0.09)	0.15	27 (2)
Ti^+	5.9 (0.5)	1.1 (0.1)	2.35 (0.10)	2.21 (0.11)	0.14	30 (3)
V^+	13.5 (0.6)	1.3 (0.1)	2.21 (0.04)	2.12 (0.07)	0.09	34 (3)
Cr^+	2.7 (1.7)	1.3 (0.1)	1.88 (0.05)	1.84 (0.06)	0.04	37 (3)
Mn^+	16.9 (1.4)	1.0 (0.1)	1.67 (0.10)	1.65 (0.10)	0.02	28 (2)
Fe^+	13.6 (0.7)	1.2 (0.1)	2.17 (0.05)	2.06 (0.08)	0.11	27 (3)
Co^+	8.9 (1.8)	1.5 (0.2)	2.74 (0.15)	2.54 (0.14)	0.20	37 (3)
Ni^+	5.8 (0.6)	1.4 (0.1)	2.71 (0.09)	2.53 (0.10)	0.18	39 (3)
Cu^+	4.4 (0.3)	1.2 (0.1)	2.79 (0.07)	2.59 (0.10)	0.20	39 (3)
Zn^+	5.0 (0.2)	1.2 (0.1)	2.27 (0.05)	2.16 (0.08)	0.11	33 (3)

[a] Uncertainties are listed in parentheses. [b] Average values for loose PSL transition state. [c] No RRKM analysis.

In most systems, the only other product that is observed in the CID reactions is the result of a ligand exchange process to form MXe^+. The cross sections for the MXe^+ products are approximately 1−2 orders of magnitude smaller than those of M^+, the primary dissociation product. For most metals, the thresholds of this cross section are slightly lower (by the M^+-Xe binding energy), although this is not always evident on the logarithmic scaled used. For a few metals (discussed further below), MXe^+ is observed at very low energies in a cross section exhibiting behavior characteristic of a near thermoneutral reaction. As little systematic information can be gleaned from these products, they will not be discussed further. However, it is conceivable that this ligand exchange process might cause a competitive shift in the observed thresholds. Within the quoted experimental errors, we do not believe such competition is likely to affect our threshold measurements in any of these systems for several reasons that have been detailed elsewhere.[38]

Additional complexity was observed with several metals (Fe^+, Co^+, and Ni^+). Specifically, a minor reaction pathway in which the reactant ion dissociates by loss of 40 amu beginning at very low energies, < 0.5 eV, was observed. Such a low-energy pathway cannot be attributed to any decomposition of the pyrimidine ligand, 80 amu. Therefore, this product can be assigned to decomposition of a small amount of $M^+(Ar)_2$, isobaric with the desired M^+(pyrimidine) complex. This assignment then provides a ready explanation for the low-energy features observed in the M^+ cross sections, which are similar in size to the M^+(Ar) product cross sections. Further, the exothermic feature in the MXe^+ cross section can now be attributed to a near thermoneutral ligand exchange process, reactions 3.

$$M^+(Ar)_2 + Xe \rightarrow MXe^+ + 2\ Ar \qquad (3)$$

As discussed above, one contribution to nonzero cross sections observed in the M^+ product data at the lowest energies can be multiple collisions. Such effects are straightforwardly removed by extrapolating the data to zero pressure of the Xe reactant. This provides cross sections for single collisions between the ion and Xe, as shown in Figure 2, behavior typical for the other M^+(pyrimidine) complexes. Even after pressure extrapolation, several of the systems examined here continue to show a nonzero cross section at kinetic energies below the CID thresholds. In these cases, the low-energy features for all ions are much smaller than the dominant cross-sectional feature (typically less than 2%), and the two features are generally distinct from one another. As noted above, these low-energy features can probably be attributed to contamination of the ion beam by $M^+(Ar)_2$, but contributions from excited states of the

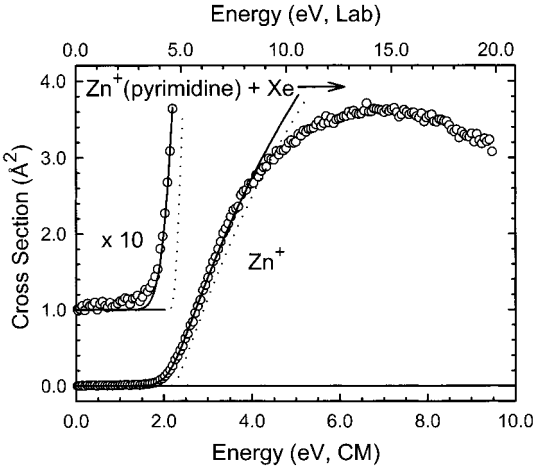

Figure 3. Zero pressure extrapolated cross section for collision-induced dissociation of the Zn^+(pyrimidine) complex with Xe in the threshold region as a function of kinetic energy in the center-of-mass frame (lower *x*-axis) and the laboratory frame (upper *x*-axis). (Note: the low-energy feature has not been subtracted.) A solid line shows the best fit to the data using eq 1 convoluted over the neutral and ion kinetic energy distributions. A dashed line shows the model cross sections in the absence of experimental kinetic energy broadening for reactants with an internal energy corresponding to 0 K.

M^+(pyrimidine) species are also possible. Similar features in the M^+ cross sections (but not alternate products or a low-energy feature in the MXe^+ cross sections) were previously observed in the CID reactions of M^+(benzene) and $M^+(benzene)_2$,[38] and M^+(pyridine) systems[9] and were attributed to electronic excitation.

Threshold Analysis. The model of eq 1 was used to analyze the thresholds for reactions 2 in 12 M^+(pyrimidine) systems. The presence of the low-energy features in many of these systems complicates the data analysis. In each case, the data are analyzed before and after subtraction of the low-energy feature (also analyzed using eq 1 with internal energies but no lifetime effect included). The reported values represent the average values determined. The variations in the measured thresholds are included in the uncertainties reported. The results of these analyses are provided in Table 1 for all 12 metal ions, and representative results are shown in Figure 3 for the Zn^+-(pyrimidine) complex. Results for all 12 metal ions are available in Figure S2 in Supporting Information. In all cases, the experimental cross sections for reactions 2 are accurately reproduced using a loose PSL TS model.[3] Previous work has shown that this model provides the most accurate assessment of the kinetic shifts for CID processes for electrostatic ion-molecule complexes.[1−4,36,37] Good reproduction of the data is

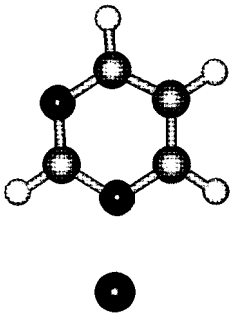

Figure 4. Optimized B3LYP/6-31G* geometry of Zn^+(pyrimidine).

obtained over energy ranges exceeding 3.0 eV and cross section magnitudes of at least a factor of 100. Table 1 also includes values of E_0 obtained without including the RRKM lifetime analysis. Comparison of these values with the E_0(PSL) values shows that the kinetic shifts observed for these systems vary from 0.02 to 0.20 eV. The total number of vibrations, 27, and heavy atoms, 7, remains the same in all of these M^+(pyrimidine) complexes, and hence the number of low-frequency vibrations remains the same. This implies that the observed kinetic shift should directly correlate with the density of states at threshold, which depends on the measured BDE. This is exactly what is found, as shown in Table 1.

The entropy of activation, $\Delta S^\dagger$, is a measure of the looseness of the TS and a reflection of the complexity of the system. It is largely determined by the molecular parameters used to model the energized molecule and the TS, but also depends on the threshold energy. Listed in Table 1, $\Delta S^\dagger$(PSL) values at 1000 K show little variation, as expected based upon the similarity of these systems, and range between 27 and 39 J mol^{-1} K^{-1} across these systems. These entropies of activation can be favorably compared to $\Delta S^\dagger_{1000}$ values in the range of 29−46 J K^{-1} mol^{-1} collected by Lifshitz for several simple bond cleavage dissociations of ions.[41]

Theoretical Results. Theoretical structures for neutral pyrimidine and for the complexes of pyrimidine with Mg^+, Al^+, Sc^+, Ti^+, V^+, Cr^+, Mn^+, Fe^+, Co^+, Ni^+, Cu^+, and Zn^+ were calculated as described above. Table S3 in Supporting Information gives details of the final geometries for each of these species. Results for the most stable conformation of the Zn^+(pyrimidine) complex is shown in Figure 4.[42] Not surprisingly, the calculations find that the metal ion prefers to be bound to the nitrogen atom rather than the π cloud of the aromatic ring of pyrimidine. This indicates that the σ interaction with the lone pair of electrons on the nitrogen atom is indeed stronger than with the π cloud. Further, because of the strong ion-dipole and ion-induced dipole interactions, the potential energy surface for M^+ + pyrimidine should be attractive such that there are no barriers in excess of the bond energy for dissociation of M^+(pyrimidine). In general, the distortion of the pyrimidine molecule that occurs upon complexation to a metal ion is minor, Table S3. The change in geometry is largest for the late transition metals. Bond lengths and angles change in the most extreme cases by less than 0.02 Å and 2.4°, respectively.

Conversion from 0 to 298 K. To allow comparison to commonly used experimental conditions, we convert the 0 K bond energies determined here to 298 K bond enthalpies and free energies. The enthalpy and entropy conversions are calculated using standard formulas (assuming harmonic oscillator and rigid rotor models) and the vibrational and rotational constants determined for the B3LYP/6-31G* optimized geometries, which are given in Tables S1 and S2. Table 2 lists 0 and 298 K enthalpy, free energy, and enthalpic and entropic corrections for all systems experimentally determined (from Table 1). Uncertainties in the enthalpic and entropic corrections are determined by 10% variation in the molecular constants. Because the metal-ligand frequencies are very low and may not be adequately described by theory, the listed uncertainties also include changing the three metal-ligand frequencies by a factor of two. The latter provides a conservative estimate of computation errors in these low-frequency modes and is the dominant source of the uncertainties listed.

Discussion

Comparison of Theory and Experiment. The metal cation affinities of pyrimidine at 0 K measured here by guided ion beam mass spectrometry are summarized in Table 3. Also listed here are the 0 K proton and metal binding energies calculated at the B3LYP/6-311+G(2d,2p)//B3LYP/6-31G* level including zero point energy corrections, and basis set superposition error corrections.[43,44] Experimental and theoretical values for proton and alkali metal ion binding to pyrimidine taken from previous studies are also provided in Table 3 for comparison.[7,45−48,] The agreement between theory and experiment for the alkali metal ions as well as those examined here is illustrated in Figure 5. It can be seen that the agreement between theory and experiment is quite reasonable over the 180 kJ/mol variation in binding affinities measured. For the 15 M^+(pyrimidine) systems, the mean absolute deviation (MAD) between experiment and B3LYP theory is 9.0 ± 5.0 kJ/mol. This is slightly larger than the average experimental error of 7.9 ± 2.6 kJ/mol. When the alkali metal ions are not included, the MAD between experiment and B3LYP theory is slightly larger and is 9.3 ± 5.5 kJ/mol, while the average experimental error is also somewhat larger, 8.4 ± 2.3 kJ/mol. The MAD between experiment and B3LYP theory for the alkali metal ions is somewhat smaller, 7.8 ± 3.1 kJ/mol. The average experimental error for the alkali metal ions is 6.2 ± 3.7 kJ/mol. Better agreement between theory and experiment is found for the alkali metal ions using MP2 theory where the MAD is 1.5 ± 1.8 kJ/mol. The higher degree of covalency expected in metal-ligand complexes involving transition metal ions suggests that accurate determination of binding

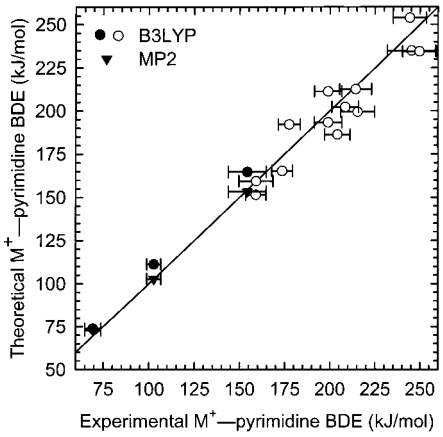

Figure 5. Theoretical versus experimental bond dissociation energies (in kJ/mol) of M^+(pyrimidine), where M^+ = Li^+, Na^+, K^+, Mg^+, Al^+, Sc^+, Ti^+, V^+, Cr^+, Mn^+, Fe^+, Co^+, Ni^+, Cu^+, and Zn^+. All values are at 0 K and taken from Table 3. Experimental (●) and MP2 (▼) values for the alkali metal ion systems are taken from Amunugama and Rodgers.[7] The diagonal line indicates the values for which calculated and measured bond dissociation energies are equal.

TABLE 2: Enthalpies and Free Energies of Metal Ion Binding of M^+(pyrimidine) at 298 K in kJ/mol[a]

M^+	ΔH_0	ΔH_0[b]	ΔH_{298} -ΔH_0[b]	ΔH_{298}	ΔH_{298}[b]	$T\Delta S_{298}$[b]	ΔG_{298}	ΔG_{298}[b]
Mg^+	173.6 (5.7)	165.3	1.3 (2.2)	174.9 (6.1)	166.6	30.5 (6.9)	144.4 (9.2)	136.1
Al^+	159.0 (5.7)	151.5	1.1 (2.1)	160.1 (6.1)	152.6	30.3 (7.0)	129.8 (9.3)	122.3
Sc^+	214.2 (8.8)	212.6	1.0 (2.0)	215.2 (9.0)	213.6	30.1 (7.0)	185.1 (11.4)	183.5
Ti^+	213.7 (10.3)	199.4	1.1 (2.2)	214.8 (10.5)	200.5	31.8 (6.9)	183.0 (12.6)	168.7
V^+	204.1 (7.0)	186.2	1.3 (2.2)	205.4 (7.3)	187.5	31.8 (6.9)	173.6 (10.0	155.7
Cr^+	177.5 (6.0)	192.1	1.3 (2.2)	178.8 (6.4)	193.4	31.9 (6.9)	146.9 (9.4)	161.5
Mn^+	159.1 (9.5)	159.4	0.8 (1.9)	159.9 (9.7)	160.2	29.9 (7.1)	130.0 (12.0)	130.3
Fe^+	199.0 (7.6)	193.2	0.8 (1.9)	199.8 (7.8)	194.0	27.5 (7.0)	172.3 (10.5	166.5
Co^+	245.1 (13.5)	234.8	1.5 (2.3)	246.6 (13.7)	236.3	32.9 (6.8)	213.7 (15.3)	203.4
Ni^+	244.2 (9.3)	253.8	1.7 (2.4)	245.9 (9.6)	255.5	33.4 (6.7)	212.5 (11.7)	222.1
Cu^+	249.6 (9.5)	234.4	1.7 (2.3)	251.3 (9.8)	236.1	33.2 (6.7)	218.1 (11.9)	202.9
Zn^+	208.4 (7.4)	202.2	1.2 (2.1)	209.6 (7.7)	203.4	31.7 (6.9)	177.9 (10.3	171.7

[a] Uncertainties are listed in parentheses. [b] Density functional theory values from calculations at the B3LYP/6-311+G(2d,2p) level of theory using B3LYP/6-31G* optimized geometries with frequencies scaled by 0.9804.

TABLE 3: Experimental and Calculated Enthalpies of Proton and Metal Ion Binding to Pyrimidine at 0 K in kJ/mol

	experiment		theory					
			MP2[c,d]			B3LYP[a,e]		
M^+	GIBMS[a]	literature[b]	D_e	D_0	$D_{0,BSSE}$	D_e	D_0	$D_{0,BSSE}$
H^+		879.9 (16.0)[f]	907.5	872.6	862.9	921.9	887.0	886.1
Li^+	154.3 (10.5)[d]	158.7 (8.4)[g]	164.3	158.9	153.3	171.3	165.6	164.7
Na^+	102.7 (3.9)[d]		111.8	108.8	102.7	116.3	113.0	111.2
K^+	69.4 (4.3)[d]		78.5	76.4	72.9	76.8	74.4	73.8
Mg^+	173.6 (5.7)					171.5	167.5	165.3
Al^+	159.0 (5.7)					156.1	152.5	151.5
Sc^+	214.2 (8.8)					218.2	214.7	212.6
Ti^+	213.7 (10.3)					203.6	200.0	199.4
V^+	204.1 (7.0)					191.2	187.3	186.2
Cr^+	177.5 (6.0)					197.0	192.9	192.1
Mn^+	159.1 (9.5)					164.9	161.7	159.4
Fe^+	199.0 (7.6)					197.0[h]	193.7[h]	193.2[h]
						215.0[i]	211.8[i]	211.3[i]
Co^+	245.1 (13.5)					240.4	235.8	234.8
Ni^+	244.2 (9.3)					259.8	254.8	253.8
Cu^+	249.6 (9.5)					241.5	236.4	234.4
Zn^+	208.4 (7.4)					208.0	204.0	202.2

[a] This work except as noted. [b] All literature values adjusted to 0 K. [c] Calculated at the MP2(full)/6-311+G(2d,2p) level of theory using MP2(full)/6-31G* optimized geometries with frequencies scaled by 0.9646 and including zero point energy and basis set superposition error corrections. [d] Amunugama and Rodgers.[7] [e] Calculated at the B3LYP/6-311+G(2d,2p) level of theory using B3LYP/6-31G* optimized geometries with frequencies scaled by 0.9804 and including zero point energy and basis set superposition error corrections. [f] Meot-Ner.[45,46] [g] Taft and co-workers.[47,48] [h] $Fe^+(s^1d^6, {}^6D)$. [i] $Fe^+(d^7, {}^4F)$.

energies for such systems might also require high levels of correlation to obtain values consistent with the experimental results obtained here. Because calculations at the level performed here were extremely time intensive with the hardware currently available to us, higher level calculations (using full MP2 correlation) to obtain reliable theoretical values were not pursued. However, the accuracy of structures and molecular parameters (vibrational frequencies and rotational constants) is not nearly as sensitive to the level of theory employed. Thus, these computational results still allow us to extract accurate thermochemical information from our experimental results.

Periodic Trends in the Binding of Metal Ions to Pyrimidine. In a previous study, the interaction of pyrimidine with the alkali metal cations was examined.[7] The bond energy is largest for Li^+ and decreases from Na^+ to K^+. This was not unexpected as this trend has been observed for a wide variety of ligands, and it can easily be explained based upon simple electrostatic ideas. Alkali metal ions have s^0 electron configurations, and therefore have spherically symmetric electron densities. The metal-ligand bond length is determined primarily by the size of the cation such that the larger the cation radius, the longer the bond and the weaker the electrostatic interaction, as observed.

The interaction of pyrimidine with the monocations examined here is not quite as simple as it is for the alkali metal ions. All of the metal ions examined here possess valence electrons. As a result, comparison of trends in the observed binding as the electron configuration is varied allows a systematic evaluation of the influence of the valence electronic structure of the metal ion. In any metal-ligand complex, the bonding between the metal ion and the ligand is dominated by three factors: the ion-dipole electrostatic attraction, the ion-induced dipole polarization attraction, and the repulsion between the metal ions valence electrons and those donated by the ligand. Ligand-to-metal donation and metal-to-ligand back-donation increases the covalent nature of the bond, whereas retention of electrons promotes ionic character in the bond. The pyrimidine ligand has three types of orbitals that it can use for bonding at the N atom. The nitrogen lone pair is a donor of electron density, occupied π orbitals may also act as donors of electron density, and the delocalized π^* antibonding orbitals may act as acceptors of electron density.

s Orbital Occupation. The series of ions, Na^+, Mg^+, and Al^+ having s^0, s^1, and s^2 occupations, respectively, allows examination of the influence of s orbital occupation upon the binding energy. As the occupation of the s orbital increases, Pauli repulsion between the electron(s) on the metal ion and the nitrogen lone pair increases, and it might be expected that the bond energies would also decrease. In contrast, the bond energies are observed to increase from Na^+ to Mg^+ and then to

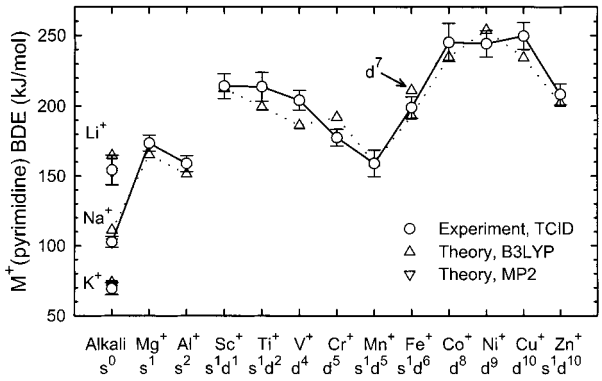

Figure 6. Experimental and theoretical bond dissociation energies (in kJ/mol) of M^+(pyrimidine), where $M^+ = Li^+$, Na^+, K^+, Mg^+, Al^+, Sc^+, Ti^+, V^+, Cr^+, Mn^+, Fe^+, Co^+, Ni^+, Cu^+, and Zn^+. All values CID (○), MP2 (▽), and B3LYP (△) are at 0 K. Experimental and theoretical results include values from Amunugama and Rodgers[7] (alkali metal ions). Ground-state electron configurations are provided for each metal ion.

decrease somewhat for Al^+, although it is still more strongly bound than Na^+. The enhancement in the bonding in the Mg^+ and Al^+ systems arises as a result of 3s-3p hybridization.[49−52] Such hybridization polarizes the electron density away from the ligand, which requires energy but exposes a higher nuclear charge to the ligand, resulting in a stronger electrostatic interaction. In the limit of complete removal of the valence electrons, this would correspond to binding to Mg^{2+} and Al^{3+}. Less enhancement of the binding in the Al^+ system is observed because electron removal is not complete, two electrons must be hybridized, and sp-hybridization requires more energy for Al^+ than for Mg^+.

s,d Orbital Occupation. Because the ionic radius of the metal decreases from left to right across the periodic table, the electrostatic contribution to bonding also increases. Therefore, the late transition metal ions generally bind more strongly than the early metal ions, as can be seen in Figure 6. Also obvious in the figure is the significant role that s,d orbital occupation plays. All of the first-row transition metal ions bind pyrimidine much more strongly (by at least a factor of 2) than K^+, the $4s^0$ ion of the same periodic row. However, strong variations in the binding across the first row indicate that the binding is influenced by other factors. Such variations have previously been explained for other metal-ligand complexes by examining the electron configuration of each of the metal ions.[9,23,53−55] These other factors arise as a result of the mechanisms by which the transition metal ion is capable of decreasing Pauli repulsion between the metal and the ligand. These mechanisms include the following: 4s-4p polarization, 4s-3dσ hybridization, and promotion to a more favorable electronic state. Because the 4p orbitals lie higher in energy than the 3d orbitals, 4s-4p polarization is more energetic than 4s-3dσ hybridization. 4s-4p polarization is analogous to the mechanism observed in the Mg^+ and Al^+ systems in that it polarizes electron density to the opposite side of the metal ion, away from the ligand, allowing the ligand to experience a larger effective nuclear charge. 4s3dσ hybridization also hybridizes electron density away from the ligand but requires less energy and places electron density in a direction perpendicular to the bonding axis. When 4s-3dσ hybridization occurs, the transition metal center exists in a combination of low-spin states having $4s^13d^n$ and $3d^{n+1}$ configurations. Therefore, the promotion energy to the higher lying of these two states must be considered no matter which (if either) of these corresponds to the ground state of the metal ion.

Promotion to an electronically excited state is a third mechanism by which Pauli repulsion can be reduced. In the discussion above, 4s-3dσ hybridization involves $3d^{n+1}$ and $4s^13d^n$ states of the same spin. The thermodynamic consequences of changing spin state to optimize metal-ligand bonding can also be observed, particularly when 4s-3dσ hybridization is not possible (e.g., when $n \geq 5$, there are no $3d^{n+1}$ states of the same spin as high-spin coupled $4s^13d^n$ states). In such cases, promotion to a state of lower spin must occur before 4s-3dσ hybridization can occur. Such promotion becomes more likely as the strength of the ligand field increases. This generally occurs as a result of multiple ligation, which is not examined here, although pyrimidine is a stronger field ligand than many of the systems previously examined.

The measured M^+−pyrimidine BDEs decrease for the early transition metals from Sc^+ to Mn^+. The ground-state electron configuration of Sc^+ is a triplet $4s^13d^1$, and promotion of the ion into a triplet $3d^2$ configuration, emptying the 4s orbital, would decrease the Pauli repulsion but requires 57.5 kJ/mol.[56] The calculated bond distance, 2.26 Å (Table S3), is the largest of all the transition metal complexes studied. For Ti^+, we find a comparable bond energy and a somewhat shorter M−N bond distance. Ti^+ has two low-lying ^4F states: a $4s^13d^2$ ground state and a $3d^3$ configuration that lies only 10.9 kJ/mol higher in energy.[56] These two states can mix to hybridize the 4s and 3dσ orbital, allowing an empty acceptor orbital. This could increase the bonding slightly at the cost of hybridization, apparently resulting in a shorter but comparably strong bond. A decrease in the BDE is observed from V^+ to Cr^+. Both bare metal ions have high-spin ground states, $3d^4$ and $3d^5$, respectively, with zero occupation of the 4s orbital. With the empty 4s orbital, the primary difference between the two is decreasing ionic radius and consequently increasing charge density, which would predict that Cr^+ would bind more tightly, opposite of that observed experimentally, but in agreement with the theoretical trend. This measured decrease is most likely the result of the high-spin $3d^5$ (^6S) configuration of Cr^+ forcing occupation of the 3dσ orbital, leading to some repulsive interactions with the pyrimidine ligand.

The Mn^+−pyrimidine BDE is the weakest of all of the first-row transition metal ions. The low BDE can be attributed to the very stable $4s^13d^5$ electronic configuration of ground-state Mn^+ (^7S). Because both the 4s and 3dσ orbitals are occupied and high-spin coupled, the Pauli repulsion between the metal and ligand is the greatest for this complex. The high-spin state of Mn^+ is incapable of 4s-3dσ hybridization without promotion. Such promotion would require a minimum of 113.3 kJ/mol to access the lowest-lying quintet electronic state, the ^5S ($4s^13d^5$) state.[56] As a result, the charge retained by the metal is the largest of all of the transition metal complexes studied, and the metal-ligand bond distance is quite large. Of the transition metal ions, only Sc^+ (which also has an occupied 4s orbital) has a longer metal-ligand bond length.

The M^+−pyrimidine BDE increases for the late transition metal ions starting from Fe^+, reaching a relatively constant value for Co^+, Ni^+, and Cu^+, and then falling off for Zn^+. The ground-state electron configurations of the Co^+, Ni^+, and Cu^+ ions have $3d^n$ populations. This allows for direct donation of the electron pair into the empty 4s orbital of the metal ion. Further, the size of the metal ion decreases with increasing d orbital population because of the stronger nuclear charge, resulting in stronger binding. This is illustrated by the three shortest M−N bonds among the various transition metal cation-pyrimidine complexes, Table S3.

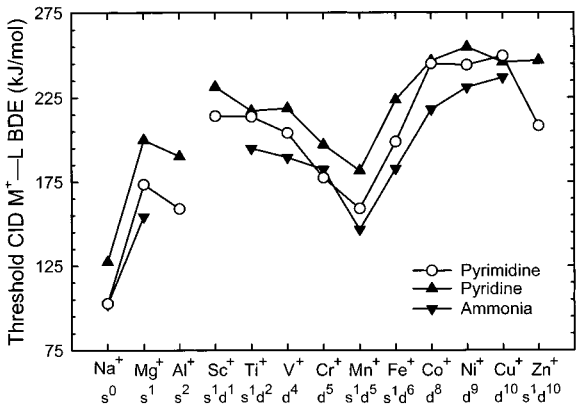

Figure 7. Comparison of the periodic trends in the M^+-L bond dissociation energies determined by collision-induced dissociation. Ligands, L, include pyrimidine (○), pyridine (▲), and ammonia (▼). Values are taken from present work and Amunugama and Rodgers,[7] Rodgers et al.,[9] and Walter and Armentrout.[57] Ground-state electron configurations are provided for each metal ion.

Iron ion has an excited state, ^{4}F, that lies only 22.4 kJ/mol above the ^{6}D ground state.[56] The excited state has a $3d^7$ configuration that should decrease the Pauli repulsion between the metal and the pyrimidine ligand. The Fe^+ bond energy is about 46 kJ/mol weaker than the Co^+ bond energy. The relative bond energies are comparable to those observed for ammonia complexes by Walter and Armentrout, where the difference is 35 ± 20 kJ/mol.[57] The weaker bond measured here lies between the theoretical values for the ^{6}D ground state and the first excited ^{4}F state, but is within experimental error of the value for the ground state. The weaker bond is either consistent with a sextet ground state (weaker because of the 4s orbital occupation and the inability to use 4s-3dσ hybridization) or with a quartet ground state (weaker because it dissociates adiabatically to the $Fe^+(^6D)$, 22 kJ/mol lower than the diabatic asymptote).

The electron configuration of Zn^+ is $4s^13d^{10}$. Occupation of the 4s orbital results in an increase in Pauli repulsion. The effect is smaller than that observed for Mn^+ as a result of the smaller size and consequently higher charge density of Zn^+. This is demonstrated by the difference in M−N bond lengths given in Table S3.

Comparison to Other Ligands. Collision-induced dissociation studies have been made of transition metal complexes with ammonia,[57] water,[23] carbonyl,[24,25,58] ethene,[59] benzene,[38] and pyridine[9] ligands. The binding energies of ammonia and pyridine show trends similar to that observed here for pyrimidine, as shown in Figure 7. The other ligands show somewhat different trends that have previously been compared to those observed in the pyridine systems.[9]

The bond between the metal ion and the ligand consists of ligand-to-metal σ electron density and π electron density. The relative ease with which a metal ion can accept the lone pair electron density changes relatively little with the ligand, but is strongest when the donor and acceptor orbitals lie closest in energy, or when more than two electrons are donated as in benzene. However, the ease of additional ligand-to-metal donation (π donor) or metal-to-ligand back-donation (π acceptor) interaction depends on both the ligand and the d-orbital population of the metal ion. If all other factors (charge density and electron polarizability of the metal ion, and dipole moment and polarizability of the ligand) are the same, then the trend in binding energies will be controlled by the d-orbital population of the metal ion, and the π donor/acceptor behavior of the ligand. For the early transition metals, with partially occupied d orbitals, binding to ligands capable of both σ and π donation is enhanced relative to that of σ donor, or σ donor and π acceptor ligands. For the late transition metals with high d-orbital occupation, a greater enhancement in binding is expected for π acceptor ligands, over σ and π donor, and σ donor ligands.

Ammonia is a σ donor, water is both a σ and π donor, carbonyl is a σ donor and π acceptor, and ethene and benzene are π donor and π acceptor ligands. On the basis of a comparison to these ligands, considering both symmetry and energy arguments, pyrimidine may participate in all three types of interactions. A σ donation interaction arises from donation of electron density from the pyrimidine $11A_1$ orbital, which is essentially the lone pair on the nitrogen atom of the ligand. A π donation interaction could involve the $2B_1$ π bonding orbital that is heavily localized on the nitrogen atom. A π acceptor interaction should be possible by donation of electron density from the metal d orbitals into the $3B_1$ π^* antibonding orbital, which is also heavily localized on the nitrogen atom. Indeed, this orbital is calculated to be more stable, (lower in energy) than the π^* acceptor orbitals on known π acceptor ligands, CO, ethene, and benzene.[60] It is therefore conceivable that the trends in the M^+-pyrimidine BDEs might parallel any of these ligands. The trends observed in the M^+-ligand BDEs to the early transition metal ions are similar for all ligands except benzene, although pyrimidine most closely parallels that of ammonia and water. The largest deviations in behavior are observed for Mn^+ and the late transition metal ions. For all ligands, the Mn^+-ligand BDE is the lowest measured of all of the transition metal ions. However, water does not show a highly pronounced dip for Mn^+, as all the other ligands do. For the late metals, the carbonyl and water trends parallel the pyrimidine in all respects, whereas ammonia, benzene, and ethene fail to track the peak in BDE for Ni^+ and decline for Cu^+.

In their study of the binding of transition metal ions to ammonia, Walter and Armentrout[57] noted distinct differences in the percent increase observed in bonding from the early to the late transition metal ions depending on whether the ligand was a π donor, π acceptor or neither. Relative to ammonia, which shows a 32% increase associated primarily with the relative sizes of the metal ions, water is a π donor and shows only a 16% increase. A much larger increase of 60% was observed for CO, a π acceptor, as expected based upon the above argument. Pyridine showed an 18% increase, whereas a 24% increase is measured here for pyrimidine (Ti−Cr vs Co−Cu). (This excludes Sc^+, which was also not included in earlier work. A 15% increase was measured for pyridine, and a 22% increase is measured for pyrimidine, when Sc^+ is included.) This is between the results for ammonia and water, and most similar to that for pyridine. This indicates that the binding in these pyrimidine complexes probably results primarily from σ donor interactions with some enhancement in binding (for the early transition metals) as a result of the π donor interaction. The larger increase seen for the late transition metals compared to pyridine suggests that the π donor interaction is not as important in the pyrimidine complexes. It is a somewhat difficult to understand why the π acceptor interaction is not more important, as the π^* antibonding orbitals are slightly lower in energy for pyridine and pyrazine than they are for CO,[60] and it can be expected that the orbital energies for pyrimidine should be very similar to those in these molecules and in particular, pyrazine.

The difference in the measured BDEs to ammonia, pyridine, and pyrimidine (Figure 7) results from the differences in the polarizability of the ligand and the extent of π back-donation.

For most metals, there is a nearly constant difference of about 15 ± 3 kJ/mol increase from ammonia to pyrimidine (excluding Sc^+, Cr^+, and Co^+, an increase of 14 ± 9 kJ/mol is measured when Cr^+ and Co^+ are included). For ammonia vs pyridine, there is a 26 ± 9 kJ/mol increase. These general trends reflect the polarizability of these three nitrogen based ligands: 2.16 Å^3 for ammonia, 8.61 Å^3 for pyrimidine, and 9.51 Å^3 for pyridine. Given the validity of these relative values for all complexes, the trends shown in Figure 7 indicate a couple of values that appear anomalous. However, it should be realized that each of these points is a completely independent experimental determination such that the experimental errors in these values easily allow the "correct" or "expected" trend to be observed. For Ti^+, either the pyrimidine value is a little high (as suggested by comparison to theory) or the pyridine value is a little low. The Cr^+ pyrimidine value appears to be low, but it is also possible that the Cr^+-NH_3 bond energy is a little lower. An alternative experimental value from Marinelli and Squires is 157 ± 19 kJ/mol,[61] 26 kJ/mol lower than the value of Walter and Armentrout used in Figure 7, and a theoretical value is 163 ± 13 kJ/mol,[62] 20 kJ/mol lower. For Co^+, the present value for pyrimidine appears to be a little high (again consistent with the theoretical trend) as the trends for pyridine and ammonia parallel one another nicely. For Cu^+, all three values are within experimental error of one another. However, the experimental value for pyrimidine is larger than for pyridine, and theory again suggests that this value may be slightly high. In our pyridine paper, we noted that Cu^+ is unable to accept any π donation from a ligand because all d orbitals are filled, whereas all earlier metal ions can. Finally, the BDE for binding Zn^+ to pyrimidine is much weaker than that for Cu^+, whereas pyridine binds approximately equally to these two metals. The trend observed here is easier to understand because of the occupation of the 4s orbital on Zn^+ (see argument for Mn^+ above). Theory also suggests that the Zn^+-pyrimidine value is quite reasonable. This difference in behavior is not understood and may indicate that the Zn^+-pyridine value is too high and should probably be remeasured.

Conclusions

The kinetic energy dependence of the collision-induced dissociation of M^+(pyrimidine), where $M^+ = Mg^+$, Al^+, Sc^+, Ti^+, V^+, Cr^+, Mn^+, Fe^+, Co^+, Ni^+, Cu^+, and Zn^+, with Xe is examined in a guided ion beam mass spectrometer. The dominant dissociation process in all cases is loss of the intact pyrimidine ligand. Thresholds for these processes are determined after consideration of the effects of reactant internal energy, multiple collisions with Xe, and lifetime effects (using methodology described in detail elsewhere).[3] Insight into the structures and binding of the metal ions to pyrimidine is provided by density functional theory calculations of these complexes performed at the B3LYP/6-311+G(2d,2p)//B3LYP/6-31G* level of theory. Reasonably good agreement between the calculated and measured values is obtained, although several of the calculated values lie outside the experimental error bars. This suggests that higher levels of correlation may be necessary to obtain accurate theoretical estimates for BDEs, particularly for the systems involving transition metal ions. However, the accuracy of structures and molecular parameters (vibrational frequencies and rotational constants) should be adequate for use in extracting accurate thermochemical information from our experimental results. The trends in measured BDEs may be explained by examining the electron population of the valence orbitals on the metal ion such that binding is the strongest for ions with d^n type configurations. Further, binding is strongest when the d orbitals are nearly full, primarily a result of the decreasing size of the metal ion with increasing d population and of π back-donation. Periodic trends in the M^+-pyrimidine BDEs are similar to those seen for ligands with similar binding modes and closely parallel those observed for ammonia, water, and pyridine ligands.

Acknowledgment. We thank P. B. Armentrout for allowing us to use the guided ion beam mass spectrometer with which these experiments were conducted. This work was supported in part by an ASMS Research Award from Micromass.

Supporting Information Available: Tables of vibrational frequencies and average vibrational energies, rotational constants, and B3LYP/6-31G* geometry optimized structures of neutral and metalated pyridine and figures showing cross sections for the collision-induced dissociation of M^+(pyrimidine) complexes (PDF). This material is available free of charge via the Internet at http://pubs/acs/org.

References and Notes

(1) Rodgers, M. T.; Armentrout, P. B. *J. Phys. Chem. A* **1997**, *101*, 1238.
(2) Rodgers, M. T.; Armentrout, P. B. *J. Phys. Chem. A* **1997**, *101*, 2614.
(3) Rodgers, M. T.; Ervin, K. M. Armentrout, P. B. *J. Chem. Phys*. **1997**, *106*, 4499.
(4) Rodgers, M. T.; Armentrout, P. B. *Int. J. Mass Spectrom*. **1999**, *185/186/187*, 359.
(5) Rodgers, M. T.; Armentrout, P. B. *J. Phys. Chem. A* **1999**, *103*, 4955.
(6) Armentrout, P. B.; Rodgers, M. T. *J. Phys. Chem. A* **2000**, *104*, 2238.
(7) Amunugama, R.; Rodgers, M. T. *Int. J. Mass Spectrom*. **2000**, *195/196*, 439.
(8) Rodgers, M. T.; Armentrout, P. B. *J. Am. Chem. Soc.* **2000**, *122*, 8548.
(9) Rodgers, M. T.; Stanley, J. R.; Amunugama, R. *J. Am. Chem. Soc* **2000**, *122*, 10969.
(10) Rodgers, M. T. *J. Phys. Chem. A* **2001**, *105*, 8145.
(11) Mátyus, P.; Fugi, K.; Tanaka, K. *Tetrahedron* **1994**, *50*, 2405.
(12) (a) Boulton, A. J.; McKillop, A. *Comprehensive Heterocyclic Chemistry*; Katritzky, A. R., Rees, C. W., Eds.; Pergamon Press: Oxford, 1984; Vol. 2, p 7. (b) Tisler, M.; Stanovnik, B. *Comprehensive Heterocyclic Chemistry*; Katritzky, A. R., Rees, C. W., Eds.; Pergamon Press: Oxford, 1984; Vol. 3, pp 2−3. (c) Porter, A. E. A. *Comprehensive Heterocyclic Chemistry*; Katritzky, A. R., Rees, C. W., Eds.; Pergamon Press: Oxford, 1984; Vol. 3, pp 158−162.
(13) Miller, K. J. *J. Am. Chem. Soc*. **1990**, *112*, 8533.
(14) Brown, D. J. *The Chemistry of Heterocyclic Compounds*, Wiley-Interscience: New York, 1962; Vol. 16, The Pyrimidines.
(15) Mó, O.; de Paz, J. L. G.; Yáñez, M. J. *Mol. Struct. (THEOCHEM)*, **1987**, *150*, 135.
(16) Sanz, J. F.; Anguiano, J.; Vilarrasa, J. *J. Comput. Chem*. **1988**, *9*, 784.
(17) Ervin, K. M.; Armentrout, P. B. *J. Chem. Phys*. **1985**, *83*, 166.
(18) Schultz, R. H.; Armentrout, P. B. *Int. J. Mass Spectrom. Ion Processes* **1991**, *107*, 29.
(19) Teloy, E.; Gerlich, D. *Chem. Phys.* **1974**, *4*, 417. Gerlich, D., Diplomarbeit, University of Freiburg, Federal Republic of Germany, 1971. Gerlich, D. In *State-Selected and State-to-State Ion−Molecule Reaction Dynamics: Part I, Experiment*; Ng, C.-Y., Baer, M. Eds. J. Wiley: New York, 1992. Gerlich, D. *Adv. Chem. Phys*. **1992**, *82*, 1.
(20) Dalleska, N. F.; Honma, K.; Armentrout, P. B. *J. Am. Chem. Soc.* **1993**, *115*, 12125.
(21) Aristov, N.; Armentrout, P. B. *J. Phys. Chem*. **1986**, *90*, 5135.
(22) Hales, D. A.; Armentrout, P. B. *J. Cluster Sci.* **1990**, *1*, 127.
(23) Dalleska, N. F.; Honma, K.; Sunderlin, L. S.; Armentrout, P. B. *J. Am. Chem. Soc.* **1994**, *116*, 3519.
(24) Schultz, R. H.; Crellin, K. C.; Armentrout, P. B. *J. Am. Chem. Soc.* **1991**, *113*, 8590.
(25) Khan, F. A.; Clemmer, D. C.; Schultz, R. H.; Armentrout, P. B. *J. Phys. Chem*. **1993**, *97*, 7978.
(26) Schultz, R. H.; Armentrout, P. B. *J. Chem. Phys*. **1992**, *96*, 1046.
(27) Fisher, E. R.; Kickel, B. L.; Armentrout, P. B. *J. Phys. Chem*. **1993**, *97*, 10204.

(28) Frisch, M. J.; Trucks, G. W.; Schlegel, H. B.; Scuseria, G. E.; Robb, M. A.; Cheeseman, J. R.; Zakrzewski, V. G.; Montgomery, J. A., Jr.; Stratmann, R. E.; Burant, J. C.; Dapprich, S.; Millam, J. M.; Daniels, A. D.; Kudin, K. N.; Strain, M. C.; Farkas, O.; Tomasi, J.; Barone, V.; Cossi, M.; Cammi, R.; Mennucci, B.; Pomelli, C.; Adamo, C.; Clifford, S.; Ochterski, J.; Petersson, G. A.; Ayala, P. Y.; Cui, Q.; Morokuma, K.; Malick, D. K.; Rabuck, A. D.; Raghavachari, K.; Foresman, J. B.; Cioslowski, J.; Ortiz, J. V.; Stefanov, B. B.; Liu, G.; Liashenko, A.; Piskorz, P.; Komaromi, I.; Gomperts, R.; Martin, R. L.; Fox, D. J.; Keith, T.; Al-Laham, M. A.; Peng, C. Y.; Nanayakkara, A.; Gonzalez, C. Challacombe, M.; Gill, P. M. W.; Johnson, B.; Chen, W. Wong, M. W.; Andres, J. L.; Gonzales, C.; Head-Gordon, M.; Replogle, E. S.; Pople, J. A. *Gaussian 98*, rev. A.9; Gaussian, Inc. Pittsburgh, PA, 1998.

(29) Foresman, J. B.; Frisch, Æ. *Exploring Chemistry with Electronic Structure Methods*, 2nd ed.; Gaussian, Inc.: Pittsburgh, PA, 1996.

(30) Beyer, T. S.; Swinehart, D. F. *Comm. Assoc. Comput. Machines* **1973**, *16*, 379. Stein, S. E.; Rabinovitch, B. S. *J. Chem. Phys.* **1973**, *58*, 2438; *Chem. Phys. Lett*. **1977**, *49*, 1883.

(31) Pople, J. A.; Schlegel, H. B.; Raghavachari, K.; DeFrees, D. J.; Binkley, J. F.; Frisch, M. J.; Whitesides, R. F.; Hout, R. F.; Hehre, W. J. *Int. J. Quantum Chem. Symp*. **1981**, *15* 269. DeFrees, D. J.; McLean, A. D. *J. Chem. Phys*. **1985**, *82*, 333.

(32) Waage, E. V.; Rabinovitch, B. S. *Chem. Rev.* **1970**, *70*, 377.

(33) Chesnavich, W. J.; Bowers, M. T. *J. Phys. Chem.* **1979**, *83*, 900.

(34) Armentrout, P. B. In *Advances in Gas Phase Ion Chemistry*; Adams, N. G., Babcock, L. M., Eds.; JAI.; Greenwich, 1992; Vol. 1, pp 83−119.

(35) See, for example: Sunderlin, L. S.; Armentrout, P. B. *Int. J. Mass Spectrom. Ion Processes* **1989**, *94*, 149.

(36) More, M. B.; Glendening, E. D.; Ray, D.; Feller, D.; Armentrout, P. B. *J. Phys. Chem.* **1996**, *100*, 1605.

(37) Ray, D.; Feller, D.; More, M. B.; Glendening, E. D.; Armentrout, P. B. *J. Phys. Chem.* **1996**, *100*, 16116.

(38) Meyer, F.; Khan, F. A.; Armentrout, P. B. *J. Am. Chem. Soc*. **1995**, *117*, 9740.

(39) See for example, Figure 1 in Dalleska et al.[20]

(40) Armentrout, P. B.; Simons, J. *J. Am. Chem. Soc.* **1992**, *114*, 8627.

(41) Lifshitz, C. *Adv. Mass Spectrom*. **1989**, *11*, 113.

(42) Figures were generated using the output of *Gaussian98* geometry optimizations in Hyperchem Computational Chemistry Software Package, ver. 5.0, Hypercube Inc., 1997.

(43) Bartlett, R. J. *Annu. Rev. Phys. Chem*. **1981**, *32*, 359.

(44) Hehre, W. J.; Radom, L.; Schleyer, P. v. R.; Pople, J. A. *Ab Initio Molecular Orbital Theory*; Wiley: New York, 1986.

(45) Meot-Ner, M. *J. Am. Chem. Soc.* **1979**, *101*, 2396.

(46) Hunter, E. P.; Lias, S. G. Proton Affinity Evaluation. In *NIST Chemistry WebBook*, NIST Standard Reference Database Number 69; Mallard, W. G., Lindstrom, P. J., Eds.; November, 1998, National Institute of Standards and Technology: Gaithersburg MD 20899. Available via the Internet at http://webbook.nist.gov.

(47) Anvia, F.; Walsh, S.; Capon, M.; Koppel, I. A.; Taft, R. W.; de Paz, J. L. G.; Catalan, J. *J. Am. Chem. Soc*. **1990**, *112*, 5095.

(48) Burk, P.; Koppel, I. A.; Koppel, I.; Kurg, R.; Gal, J.-F.; Maria, P.-C.; Herreros, M.; Notario, R.; Abboud, J.-L. M.; Anvia, F.; Taft, R. W. *J. Phys. Chem. A* **2000**, *104*, 2824.

(49) Bauschlicher, C. W., Jr.; Langhoff, S. R.; Partridge, H. *J. Chem. Phys.* **1991**, *94*, 2068.

(50) Bauschlicher, C. W.; Langhoff, S. R.; Partridge, H.; Rice, J. E.; Komornicki, A. *J. Chem. Phys.* **1991**, *95*, 5142.

(51) Bauschlicher, C. W.; Partridge, H. *J. Phys. Chem.* **1991**, *95*, 9694.

(52) Bauschlicher, C. W.; Sodupe, M.; Partridge, H. *J. Chem. Phys.* **1992**, *96*, 4453.

(53) Rosi, M.; Bauschlicher, C. W. *J. Chem. Phys*. **1989**, *90*, 7264.

(54) Rosi, M.; Bauschlicher, C. W. *J. Chem. Phys*. **1990**, *92*, 1876.

(55) Armentrout, P. B. *Acc. Chem. Res*. **1995**, *28*, 430.

(56) Sugar, J.; Corliss, C. *J. Phys. Chem. Ref. Data* **1985**, *14*, Suppl. 2, 1.

(57) Walter, D.; Armentrout, P. B. *J. Am. Chem. Soc*. **1998**, *120*, 3176.

(58) Sievers, M. R.; Armentrout, P. B. *J. Phys. Chem.* **1995**, *99*, 8135. Goebel, S.; Haynes, C. L.; Khan, F. A.; Armentrout, P. B. *J. Am. Chem. Soc.* **1995**, *117*, 6994. Khan, F. A.; Steele, D. A.; Armentrout, P. B. *J. Phys. Chem.* **1995**, *99*, 7819. Meyer, F.; Chen, Y.-M.; Armentrout, P. B. *J. Am. Chem. Soc.* **1995**, *117*, 4071.

(59) Sievers, M. R.; Jarvis, L. M.; Armentrout, P. B. *J. Am. Chem. Soc.* **1998**, *120*, 1891.

(60) Jorgensen, W. L.; Salem, L. *The Organic Chemist's Book of Orbitals*; Academic Press: New York, 1973.

(61) Marinelli, P. J.; Squires, R. R. *J. Am. Chem. Soc*. **1989**, *111*, 4101.

(62) Langhoff, S. R.; Bauschlicher, C. W.; Partridge, H.; Sodupe, M. *J. Phys. Chem.* **1991**, *95*, 10677.